Journal of Dental Research
2021, Vol. 100(10) 1099–1108

DOI: 10.1177/00220345211026838
journals.sagepub.com/home/jdr

Biomineralization of Dental Tissues Treated with Silver Diamine Fluoride

R.M. Sulyanto[1,2*], M. Kang[3*], S. Srirangapatanam[3,4], M. Berger[1,2], F. Candamo[2], Y. Wang[3], J.R. Dickson[5], M.W. Ng[1,2], and S.P. Ho[3,4]

Abstract

Silver diamine fluoride (SDF) is a dental biomaterial used to arrest dental caries. To better understand SDF's mechanism of action, we examined the localization of silver within the tissues of SDF-treated teeth. Carious primary teeth fixed within 2 min of SDF application (SDF-minutes, $n = 3$), at 3 wk after SDF application in vivo (SDF-weeks, $n = 4$), and at 2 y after multiple SDF applications in vivo (SDF-multiple, $n = 1$) were investigated in this study. Carious primary teeth without SDF application (no-SDF, $n = 3$) served as controls. Mineral density and structural analyses were performed via micro–X-ray computed tomography and scanning electron microscopy. Elemental analyses were performed through X-ray fluorescence microprobe and energy-dispersive X-ray spectroscopic techniques. SDF-treated teeth revealed higher X-ray–attenuated surface and subsurface regions within carious lesions, and similar regions were not present in no-SDF teeth. Regions of higher mineral density correlated with regions of silver abundance in SDF-treated teeth. The SDF penetration depth was approximated to 0.5 ± 0.02 mm and 0.6 ± 0.05 mm (mean $\pm$ SD) for SDF-minutes and SDF-weeks specimens, respectively. A higher percentage of dentin tubular occlusion by silver or calcium phosphate particles was observed in primary teeth treated with SDF-weeks as compared with SDF-minutes. Elemental analysis also revealed zinc abundance in carious lesions and around the pulp chamber. SDF-weeks teeth had significantly increased tertiary dentin than SDF-minutes and no-SDF teeth. These results suggest that SDF treatment on primary teeth affected by caries promotes pathologic biomineralization by altering their physicochemical properties, occluding dentin tubules, and increasing tertiary dentin volume. These seemingly serendipitous effects collectively contribute to the cariostatic activity of SDF.

Keywords: caries, tertiary dentin, primary tooth, trace metals, zinc, metalloprotease

Introduction

Silver diamine fluoride (SDF) is a dental biomaterial that is used as a cariostatic agent and as a treatment for dentin hypersensitivity (Crystal and Niederman 2019). Topical application of SDF to carious lesions can be performed in a few minutes without the need for anesthetics or sedatives (Horst et al. 2016), and the use of SDF is a key strategy in minimally invasive dentistry, particularly in the pediatric population (Frencken et al. 2012). In 2017, the American Academy of Pediatric Dentistry provided evidenced-based recommendations for the use of 38% SDF to arrest cavitated carious lesions on primary teeth (Crystal et al. 2017) but highlighted the need for further studies to understand the cariostatic efficacy of SDF.

Despite the clinical effectiveness of SDF in arresting caries (Chu et al. 2002; Llodra et al. 2005; Yee et al. 2009; Zhi et al. 2012; Crystal et al. 2017; Slayton et al. 2018; Urquhart et al. 2019), the mechanism of SDF action is not fully understood (Zhao et al. 2018). The traditional understanding is that the silver component of SDF provides antibacterial activity while the fluoride component helps remineralize the carious dentin (Crystal and Niederman 2019). In vitro, ex vivo, and in vivo research, however, has suggested a more complex and nuanced mechanism of action of SDF. SDF effects on dentin have primarily been studied with ex vivo models. It has been suggested that silver compounds occluded dentinal tubules in carious lesions and in turn inhibited the progression of microbial species into

[1]Department of Dentistry, Boston Children's Hospital, Boston, MA, USA
[2]Department of Developmental Biology, Harvard School of Dental Medicine, Boston, MA, USA
[3]Department of Preventive and Restorative Dental Sciences, School of Dentistry, University of California San Francisco, San Francisco, CA, USA
[4]Department of Urology, School of Medicine, University of California San Francisco, San Francisco, CA, USA
[5]Department of Neurology, Massachusetts General Hospital and Harvard Medical School, Boston, MA, USA
*Authors contributing equally to this article

A supplemental appendix to this article is available online.

Corresponding Author:
S.P. Ho, Division of Preclinical Education, Biomaterials and Engineering, Department of Preventive and Restorative Dental Sciences, D 3210, School of Dentistry, University of California San Francisco, 707 Parnassus Avenue, San Francisco, CA 94143, USA.
Email: sunita.ho@ucsf.edu

dentin, thereby preventing acid diffusion through the tubules (Shah et al. 2014). Metallic silver and silver chloride have been found in dentin specimens treated with SDF (Mei et al. 2012; Yu et al. 2018). Specifically, silver was observed in dentin tubules in isolated dentin or enamel specimens treated with SDF (Yu et al. 2018; Sayed et al. 2019) and in extracted teeth treated with SDF ex vivo (Willershausen et al. 2015; Seto et al. 2020). Recent studies also examined the interaction of the silver component of SDF with dentin. SDF has been shown to react with hydroxyapatite to form calcium fluoride, fluoroapatite, and insoluble silver phosphate, thereby increasing dentin hardness and resistance to acid dissolution or demineralization (Suzuki et al. 1974; Shah et al. 2014). SDF has additionally been shown to inhibit the function of matrix metalloproteases (MMPs). MMPs degrade collagen in dentin, and loss of their function is thought to facilitate dentin remineralization (Zhao et al. 2018).

Few studies have reported examination of SDF-treated carious lesions in vivo and subsequent examination of these teeth following exfoliation or extraction (Mei et al. 2014; Bimstein and Damm 2018). We hypothesized that the interaction of SDF with carious lesions could produce favorable alterations in the demineralized carious tissue in a time-dependent manner. To test this hypothesis, we examined the effect of SDF application on the structure and elemental composition of dentin of carious primary teeth at 3 time points. Spatial maps of mineral density (MD) were correlated with elements colocalized on affected carious dentin. Carious tooth structure was visualized using high-resolution electron microscopy and X-ray spectroscopy techniques.

Materials and Methods

Specimen Collection

Specimens were collected from patients at Boston Children's Hospital via an Institutional Review Board–approved protocol (IRB-P00025055). Patients aged 3 through 10 y with cavitated carious lesions in primary teeth were recruited for this prospective study. Inclusion criteria were as follows: American Society of Anesthesiology I or II, carious primary teeth that were asymptomatic or had signs of reversible pulpitis only, and caries that were directly accessible without removal of tooth structure with a dental handpiece. No unhealthy patients were included in this study because of potential confounders (American Society of Anesthesiology III or higher). Exclusion criteria were patients with caries extending to the pulp. A total of 11 carious primary teeth were included in the study: SDF untreated (no-SDF, $n = 3$), one-time SDF treated 2 min prior to planned extraction (SDF-minutes, $n = 3$), one-time SDF treated 3 wk prior to planned extraction (SDF-weeks, $n = 4$), and SDF treated 5 times over a 2-y period prior to ultimate extraction (SDF-multiple, $n = 1$). SDF (Advantage Arrest) was applied for 60 s during each application per the usual clinical protocol followed by the dental department at Boston Children's Hospital based on guidelines from the American Academy of Pediatric Dentistry ("Chairside Guide" 2018). Clinical radiographs were obtained prior to tooth extraction in the course of routine clinical care (Fig. 1). Teeth were fixed in 10% neutral formalin solution and processed for laboratory analysis.

MD Analyses with Micro X-ray Computed Tomography

With micro X-ray computed tomography (μXCT; MicroXCT-200 [Carl Zeiss Microscopy]), specimens were imaged at 2 magnifications: 2× (pixel size, 10 μm) and 4× (pixel size, 5 μm) at 80 kVp and 40 kVp of energy, respectively. The reconstructed images of the specimens were analyzed with AVIZO 2019.2 software (Fisher Scientific). Volumes of carious tooth structure and tertiary dentin were measured after segmentation based on X-ray intensity and structure. X-ray intensity values were converted to MD (mg/mL) following a published calibration protocol (Djomehri et al. 2015). The MD profiles of regions of interest of selected specimens were plotted with Fiji (Schindelin et al. 2012). The estimated volumes of tertiary dentin from the 2 groups were compared with an unpaired t test: no-SDF and SDF-minutes (total $n = 4$) versus SDF-weeks ($n = 4$).

Elemental Mapping with X-ray Fluorescence Microprobe

Whole specimens were sectioned along a mesial-distal plane through the carious lesion with a slow speed saw. Elemental maps, including phosphorus (P), calcium (Ca), zinc (Zn), and silver (Ag), were collected with an X-ray fluorescence microprobe (μXRF) at beamline 10.3.2 of Advanced Light Source at Lawrence Berkeley National Laboratory. Elemental distribution maps were collected with an incident beam energy of 10 keV and a spot size of ~20 × 20 μm.

Surface Morphology and Elemental Composition Analyses with FESEM and Energy-Dispersive X-ray Spectroscopy

Following μXRF, the sectioned specimens were imaged with FESEM (field emission scanning electron microscopy; SIGMA VP500 Carl Zeiss Microscopy) at various magnifications at 1 keV to obtain secondary electron (SE) images. Additional elemental analyses were performed with an energy-dispersive X-ray mode (Quantax EDS; Bruker Nano Inc.) to collect elemental maps and spectra of carbon (C), oxygen (O), fluorine (F), P, Ca, and Ag at 15 keV with a variable pressure mode. Backscattered electron (BSE) micrographs were also collected at 15 keV to delineate chemical compositions.

Colocalization and Correlative Image Analyses of MD and Elemental Maps and Immunolocalized Biomolecules

For spatial correlation of MD and elemental (P, Ca, Zn, Ag) maps, 5 to 20 X-ray tomograms (number of tomograms

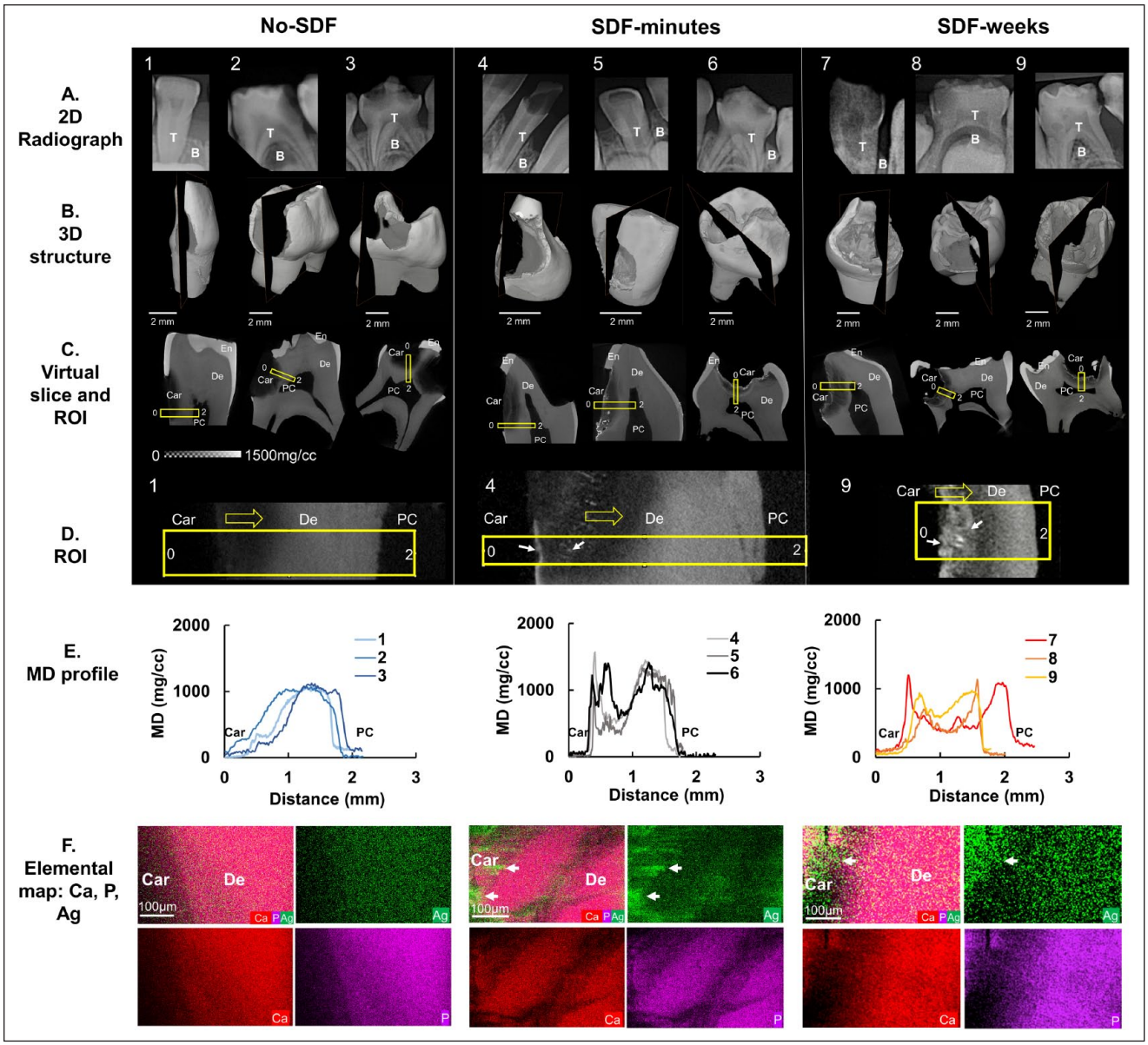

Figure 1. Mineral density (MD) and elemental maps of silver diamine fluoride (SDF)–treated carious teeth. Nine carious primary teeth in 3 treatment groups were evaluated: no-SDF (teeth 1 to 3), SDF-minutes (teeth 4 to 6), and SDF-weeks (teeth 7 to 9). (**A**) Two-dimensional (2D) clinical X-ray radiographs, (**B**) 2D slices within 3-dimensional (3D) volume-rendered structures, and (**C**) corresponding 2D virtual slices/tomograms in each treatment group. (**D**) Region of interest (ROI; yellow rectangular box) in each 2D slice for all 9 teeth examined by an energy-dispersive X-ray unit. Representative regions span the carious surface (0) to the pulp chamber (2) for teeth 1, 4, and 9 (yellow arrows, direction; white arrows, Ag). (**E**) Heterogenous MD profiles along the length of the ROI for each tooth obtained by micro X-ray computed tomography are illustrated. (**F**) Elemental spatial maps of Ca, P, and Ag (white arrows) of representative ROIs for each treatment group were obtained by energy-dispersive X-ray. B, bone; Car, caries; De, dentin; PC, pulp chamber; T, teeth.

depended on specimen size) were selected and averaged to account for the μXRF penetration depth. Tomograms displaying average MD were then translated, rotated, scaled, and cropped to register with corresponding elemental maps with Avizo. Registered MD and elemental maps were analyzed with Fiji (Schindelin et al. 2012) for colocalization of elements and subsequent correlation of colocalized elements with MDs. Regions above mean counts of each element were segmented and overlaid on MD maps to colocalize elements within lower and higher MD regions. Spatial association between elements was also analyzed with correlative maps (see Appendix S1 File). Further data analyses and visualization were performed in R version 3.6.3 (R Core Team 2020). Two-dimensional correlative plots of MD-Zn, P-Zn, Ca-Zn, and Ag-Zn were obtained to identify the spatial association of elemental Zn with other elements and in lower and higher MD regions. Higher and lower Zn regions were segmented with a threshold of mean counts. Binary masks corresponding to higher and

lower Zn regions were generated with Fiji, and these masks were used to generate separate maps of MD, P, Ca, and Ag corresponding to higher and lower Zn regions. Histograms and box plots of MD, P, Ca, and Ag within higher Zn and lower Zn regions were obtained (see Appendix S2 File). Dentin matrix protein 1 (DMP-1) and MMP-13 were immunolocalized in SDF-treated specimens (see Appendix for details). Spatial correlation of MMP-13 with Zn expression in tertiary dentin in SDF-weeks carious specimen was performed.

Results

MD and Elemental Maps of Carious Teeth Treated with SDF

The severity of carious lesions and strata of different MDs within carious lesions were illustrated by the following:

- 2-dimensional clinical X-ray radiographs (Fig. 1A)
- 3-dimensional volume-rendered structures reconstructed from 2-dimensional projections of specimens scanned with μXCT (Fig. 1B)
- 2-dimensional virtual cuts within 3-dimensional structures of SDF-untreated teeth (no-SDF, teeth 1 to 3) and one-time SDF-treated teeth that were extracted after 2 min of treatment (SDF-minutes, teeth 4 to 6) and 3 wk of treatment (SDF-weeks, teeth 7 to 9; Fig. 1C, D).

At a higher magnification, the SDF-treated specimens showed higher MD near the lesion with brighter particles, whereas the untreated lesions did not contain these particles. Quantification of MD profiles (Fig. 1E) of these regions from the carious surface to pulp illustrated a gradual increase in MD in no-SDF specimens. This MD profile of no-SDF primary teeth contrasted with short but sharp multiple peaks near caries in SDF-minutes and 2 dominant peaks in SDF-weeks. Elemental spatial maps of representative regions of interest in no-SDF, SDF-minutes, and SDF-weeks specimens (Fig. 1F) illustrated distributions and colocalization of Ca, P, and Ag elements. Higher Ag content was observed in SDF-treated carious lesions. Ag in SDF-minutes was localized to higher MD zones at the outer margins of the carious lesion as compared with a subsurface localization that was observed in primary teeth treated with SDF for weeks. Higher MD peaks also illustrated higher Ca, P, or Ag in carious regions.

Distributions of Elemental Ca, P, Zn, and Ag and MD Depth Profile of Carious Teeth

MD from μXCT and elemental maps of Ca, P, Zn, and Ag from μXRF of SDF-minutes and SDF-weeks are shown in Figure 2A and 2B. SDF-minutes illustrated smaller and brighter particles of dispersed Ag particles. SDF-weeks illustrated Ag in tubules. The SDF penetration depths in SDF-minutes and SDF-weeks were ~0.5 ± 0.02 and ~0.6 ± 0.05 mm (mean ± SD), respectively (Fig. 2C, D). Higher-intensity peaks of Ca and P (light blue arrows) within carious lesions indicated less demineralized areas or a potentially remineralizing region. Some higher MD regions contained higher counts of P compared with Ca (light purple arrow), and Zn was relatively higher in these regions (light purple area, Fig. 2D).

Morphology and Spatial Distribution of Silver in Carious Primary Teeth

Backscattered electron and SE scans of a representative tooth from each treatment group were obtained at various magnifications, and Ag particles and patches (white arrows, Fig. 3) were observed. Atomic percentages of each element (P, Ca, C, O, Ag, N, F, S, Na, Mg) within each region (Fig. 3; obj 1 to 5) were obtained with energy-dispersive X-ray spectroscopy (EDX). In SDF-minutes specimens, most Ag particles accumulated within intertubular dentin alongside bacteria (Fig. 3A). In SDF-weeks, larger Ag particles and patches were observed within the carious lesion (Fig. 3B). Multiple dentin tubules were occluded by Ag (obj 4), while others were occluded by calcium phosphate (obj 3). The average size of Ag particles measured with BSE scans was 0.25 ± 0.08 μm, and Ag patches were up to 1 mm long. A greater percentage of tubules were occluded with Ag in SDF-weeks (~20%) as compared with SDF-minutes (~6%). Infiltration of Ag particles along the length of the tubules after multiple applications of SDF is shown in Figure 3C.

Colocalization of Zn, P, Ca, and Ag in Regions of Known MD

Spatial maps of MD with each element of SDF-minutes and SDF-weeks are shown in Figure 4. Regions with elemental counts above mean values were segmented (Fig. 4B, H). The resulting spatial maps of elements were overlaid with MD maps (Fig. 4C, I). Two distinct regions of higher Zn concentrations in lower and higher MD regions were observed within all specimens regardless of SDF treatment. Higher Zn counts were observed in carious dentin and around the pulp chamber (Fig. 4D, J). Zn counts were much lower in sound dentin and inside the pulp chamber of the same tooth. Scatter plots illustrate higher and lower Zn regions (Fig. 4E, K). Broad peaks from lower-to-higher MD, Ca, and P were observed within higher Zn regions, and sharp peaks at higher MD, Ca, and P were observed at lower Zn regions (Fig. 4F, L).

Tertiary Dentin in Carious Primary Teeth

Spatial correlation of MMP-13 with Zn expression in tertiary dentin in SDF-weeks carious specimen is illustrated in Appendix Figure 1. Volumes of carious teeth were segmented into different volumes of carious lesions and tertiary dentin inside the pulp chamber (Fig. 5A, B). μXRF elemental spatial maps illustrated higher Zn expressions within carious and tertiary dentin regions located around and inside the pulp chamber. Volume estimates of tertiary dentin were plotted against

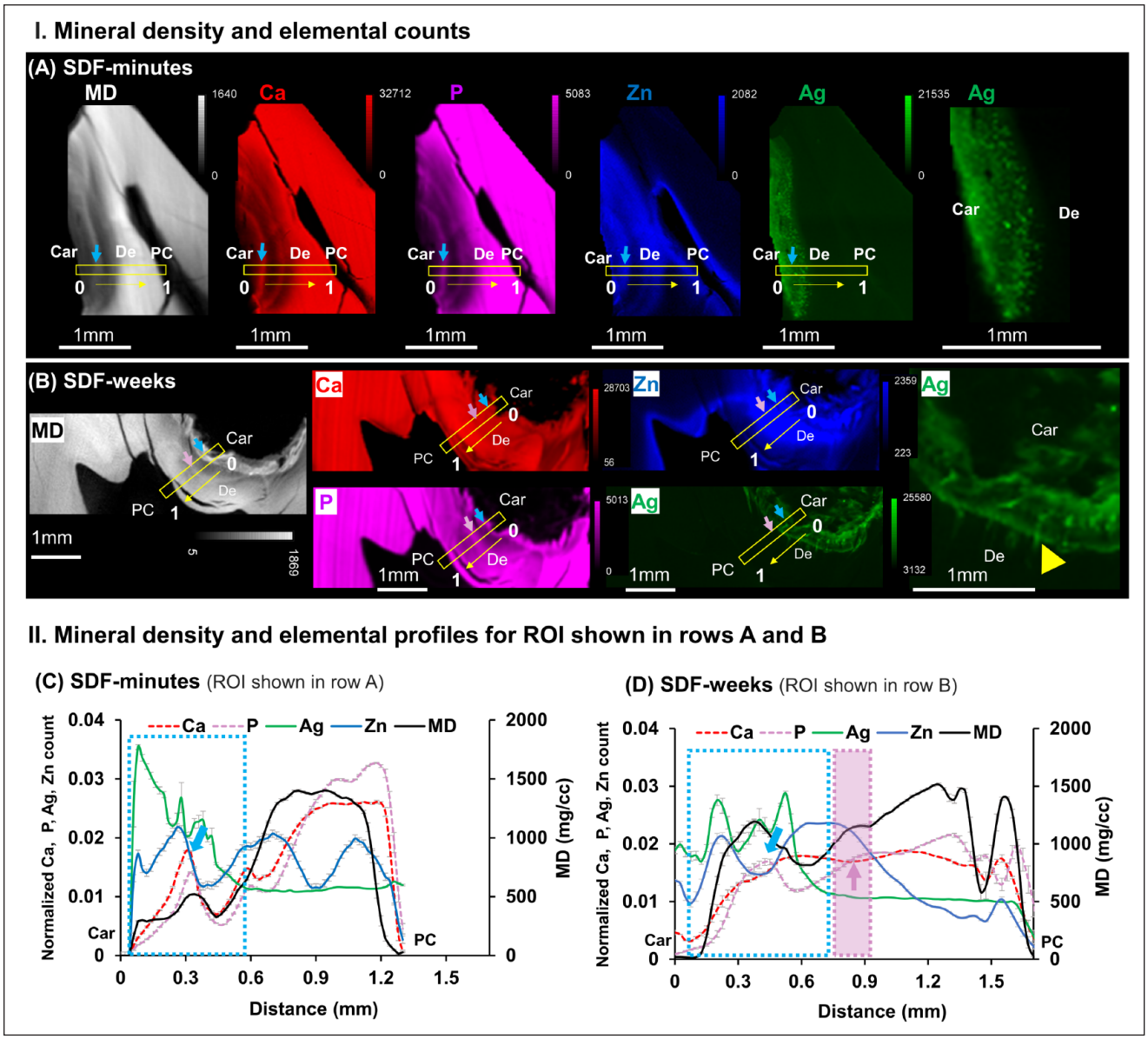

Figure 2. Varied distributions of elemental Ca, P, Zn, and Ag "shaped" the mineral density (MD) profiles unique to carious lesions treated with SDF-minutes and SDF-weeks. MD (white) from micro X-ray computed tomography and X-ray fluorescence microprobe elemental maps of Ca (red), P (pink), Zn (blue), and Ag (green) in carious primary teeth treated with a onetime SDF application and extracted (**A**) 2 min after application (SDF-minutes, tooth 4) and (**B**) 3 wk after application (SDF-weeks, tooth 9). Right-most panel shows Ag distribution at a higher magnification for both treatment groups and indicates Ag distribution along the length of the dentinal tubules in the SDF-weeks group (yellow arrowhead). MD and elemental profiles for regions of interest (ROIs; yellow boxes) from the carious margin (0) to the pulp chamber (1) in panels A and B are shown for teeth treated with SDF for (**C**) minutes (tooth 4) and (**D**) weeks (tooth 9). SDF penetration depth (light blue dotted rectangle) was estimated by spatially correlating the MD profile with that of the Ag and Ca elemental profiles. The penetration depths of SDF-minutes and SDF-weeks were ~0.5 ± 0.02 mm and ~0.6 ± 0.05 mm (mean ± SD), (yellow arrows, direction; white arrows, location of Ag particles) respectively. Ca and P peaks (light blue arrows) within carious lesions indicated potentially remineralized areas. Increased P counts with decreased Ca counts (light purple arrow within purple rectangle) were observed. Car, caries; De, dentin; PC, pulp chamber; SDF, silver diamine fluoride.

volume estimates of carious tooth structure for no-SDF, SDF-minutes, SDF-weeks, and SDF-multiple (Fig. 5C). Unpaired *t* test indicated significantly thicker tertiary dentin in teeth treated with SDF over time ($P = 0.04$ with 95% CI). BSE and SE imaging of carious lesions treated with SDF multiple times illustrated spherulitic calcified structures within the pulp chamber (orange box) characteristic of tertiary dentin (Fig. 5D). EDX maps illustrated relatively lower Ca and P atomic percentages in less mineralized (obj 2) and least mineralized (obj 3) areas as compared with tubular sound dentin (obj 1, Fig. 5E).

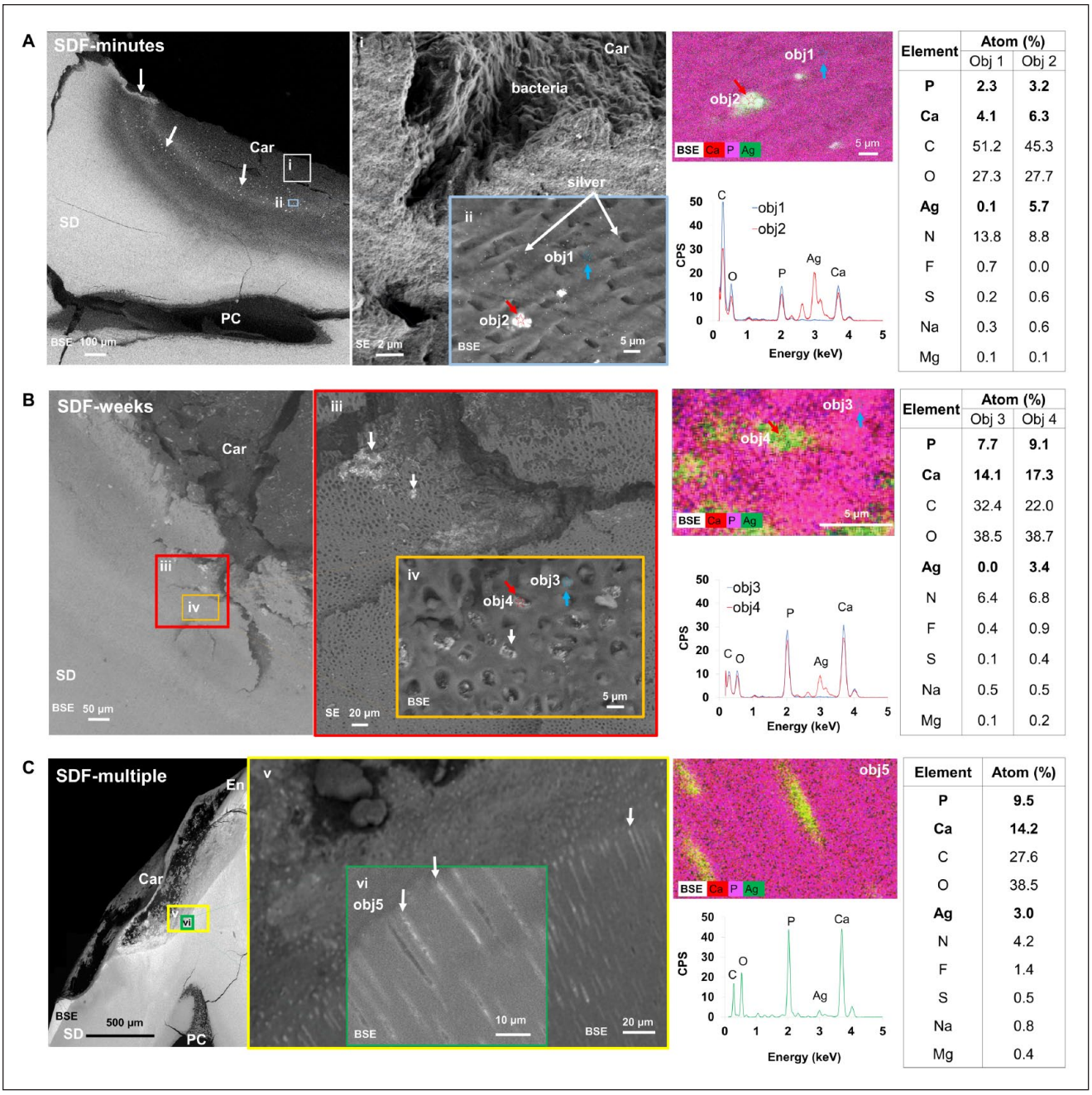

Figure 3. Morphology and spatial distributions of silver (Ag) in primary teeth affected with caries. Teeth shown are from 3 treatment groups: (**A**) SDF-minutes, (**B**) SDF-weeks, and (**C**) SDF-multiple. Backscattered electron (BSE) and secondary electron (SE) images of a representative tooth in each treatment group were obtained at various magnifications (i–vi). Grayscale differences in BSE micrographs represent variations per the atomic number of elements within regions of varying mineral densities and Ag particles (white arrows). Energy-dispersive X-ray spectra of the same regions with atomic percentages of each element in specific regions (obj 1, 2, 3, 4, 5) are presented in corresponding tables. Obj 1 to 4 were collected at a spot size of 1 µm whereas Obj 5 was obtained from an area of 828 µm^2. Objs 1 & 3, blue arrows; Objs 2 & 4, red arrows. Car, caries; En, enamel; PC, pulp chamber; SD, sound dentin; SDF, silver diamine fluoride.

Discussion

This study highlights the key changes that occur following SDF application in carious primary teeth. The effect of SDF spans the carious dentin surface to the pulp chamber and contributes to changes in the physiochemical properties of the tooth.

The MD profile (Fig. 1) spanning the carious margin to the pulp was heterogeneous. In untreated carious teeth, MD was lowest at the carious margin, attributable to demineralization

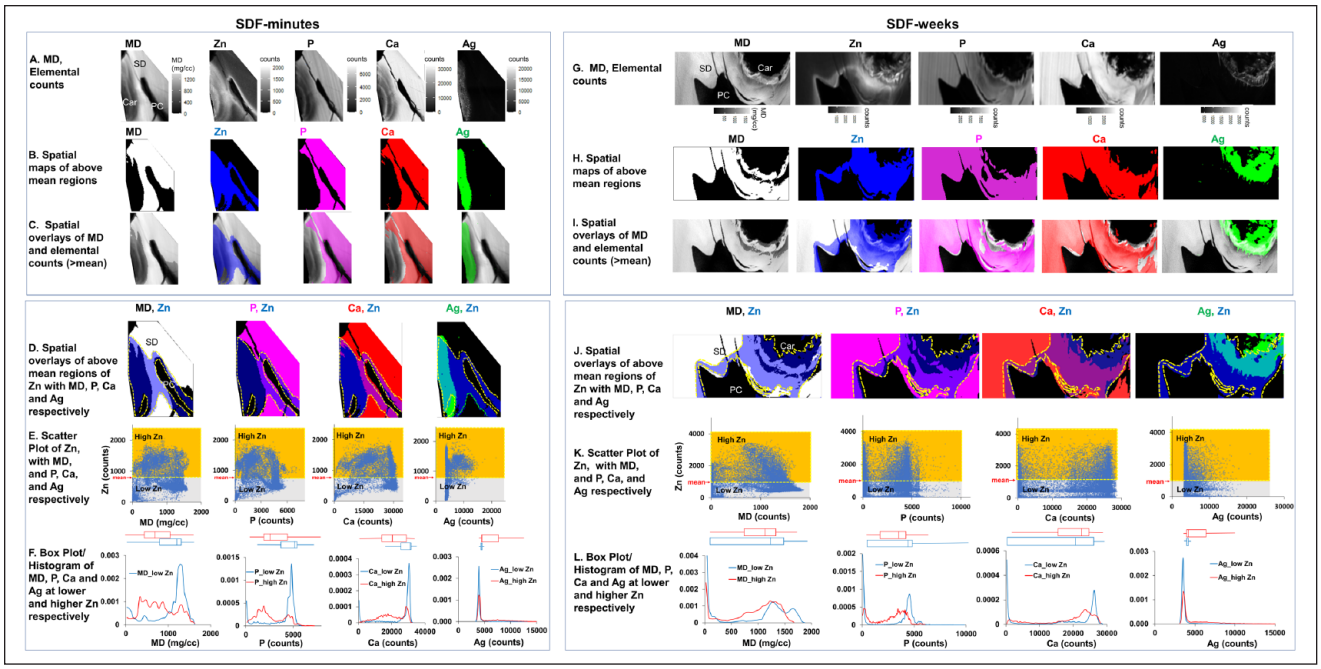

Figure 4. Colocalization of zinc (Zn), phosphorus (P), calcium (Ca), and silver (Ag) in regions of known mineral densities (MDs) and spatial correlation between Zn and MD, Zn and Ca, Zn and P, and Zn and Ag in SDF-treated primary teeth. Spatial maps of MD and each element of SDF-minutes (**A–F**) and SDF-weeks (**G–L**) are shown. Regions with MD or elemental counts above mean values were segmented (B, H), and resulting elemental distribution maps were overlaid with MD maps (C, I). Higher Zn counts (above mean represented by yellow dotted line) were observed in carious dentin and around the pulp chamber (D, J). Scatter plots (E, K) illustrate higher (yellow) and lower (gray) Zn regions, and box plots and histograms of MD, Ca, P, and Ag within higher (red line) and lower (blue line) Zn regions are shown (F, L). Car, caries; PC, pulp chamber; SD, sound dentin; SDF, silver diamine fluoride.

associated with caries, and gradually increased to a peak at sound dentin. In SDF-treated teeth, an elevated MD at the carious surface paralleled the appearance of radiopaque borders along the outer caries margin where SDF was applied. EDX mapping confirmed that this radiopaque border was attributable to increased silver particle accumulation in areas of greatest dentin denaturation. Larger aggregates accumulated superficially at the outer carious margin, while smaller silver particles were observed deeper and farther away from the carious lesion. The notable increase in radiopacity observed within minutes of SDF application, as well as weeks after application at the outermost carious margin, suggests the immediate formation of a hard barrier. This barrier may impede the progression of cariogenic microbes or their metabolites into dentin. The depth of silver penetration along dentinal tubules poses important implications for the efficacy of SDF-mediated caries arrest and pulpal response. Based on µXRF elemental analysis (Fig. 2), silver accumulation within minutes of application was observed to a depth of ~0.5 mm, increasing to ~0.6 mm after 3 wk. While a majority of silver penetration along dentin tubules appears to occur within minutes after application, the increase in SDF penetration depth and tubule occlusion after 3 wk suggests a time-dependent process. BSE and SE analyses illustrated accumulation of silver-rich particles on intertubular dentin after minutes of application and particles within tubular dentin after 3 wk of SDF treatment. Diffusive and capillary forces may contribute to fluid flow within tubules over time. Pashley and Matthews (1993) described diffusion across 1 to 2 mm of healthy dentin to take 30 to 120 min with in vitro studies. Additionally, directionality of dentin tubules and dentin permeability may contribute to penetration depth (Li et al. 2019). The mean depth of silver penetration in this study is consistent with previous studies (Li et al. 2019; Seto et al. 2020), with variability likely resulting from differences in study design.

The significantly higher volume of tertiary dentin observed by µXCT in SDF-treated primary teeth over time suggests an SDF-mediated reactive or reparative dentin process (Larmas and Sándor 2014). Tubular dentin occluded by silver particles and mineralized structures rich in Ca and P in all SDF-treated specimens (Fig. 3) illustrated an extrinsic and intrinsic adaptation of dentinal tissue to microbial insult. A thin but higher MD tissue is evident along the coronal pulp of untreated carious primary teeth, which is characteristic of tertiary dentin deposited in response to chronic infectious stimuli (Klinge 2001). A 3-dimensional examination of the full volume of carious lesion and temporal comparison at 3 time points illustrated that the promotion of a reparative process is a relatively early effect of SDF application (i.e., within a few weeks). Globular calcospherites rich in Ca and P occupied the coronal predentin region of carious primary teeth (Fig. 5), a phenomenon that has been linked to secretory activity of the predentin during secondary dentinogenesis (Mishima and Kozawa 1998). Kirk and Meyer (1992) described formation of calcospherites as a reparative process following calcium hydroxide treatment of exposed pulps in rat incisors. These findings support clinical observations of SDF as an indirect pulp-capping agent and are

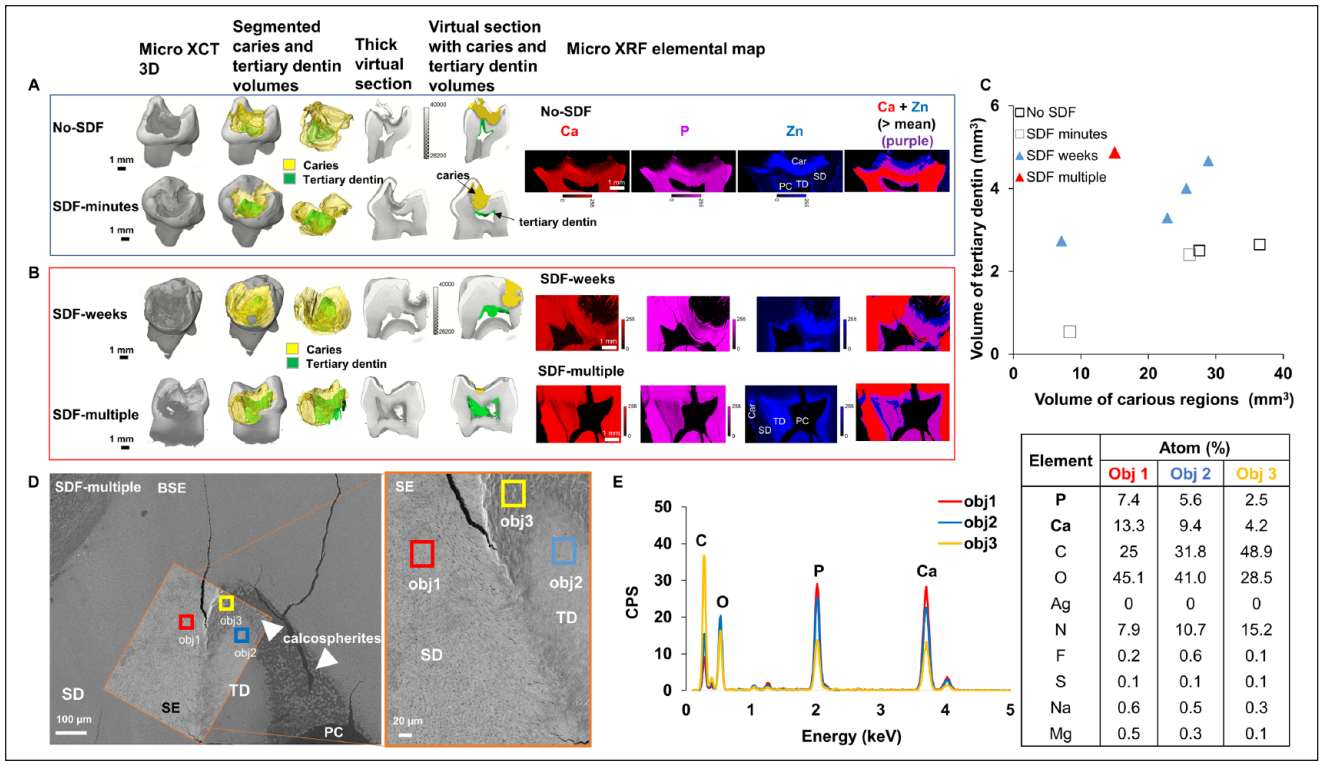

Element	Atom (%)		
	Obj 1	Obj 2	Obj 3
P	7.4	5.6	2.5
Ca	13.3	9.4	4.2
C	25	31.8	48.9
O	45.1	41.0	28.5
Ag	0	0	0
N	7.9	10.7	15.2
F	0.2	0.6	0.1
S	0.1	0.1	0.1
Na	0.6	0.5	0.3
Mg	0.5	0.3	0.1

Figure 5. Tertiary dentin in SDF-treated primary teeth. (**A**, **B**) Three-dimensional volume-rendered images and virtual sections overlaid with mineral density segmented volumes illustrate different volumes of carious lesions (yellow) and tertiary dentin (green) inside the pulp chamber. X-ray fluorescence microprobe elemental distribution maps demonstrate Ca (red), P (pink), and Zn (blue) expressions within carious and tertiary dentin regions located around and inside the pulp chamber. (**C**) Volume estimates of tertiary dentin were plotted against volume estimates of carious lesions for carious primary molars not treated with SDF, treated with SDF for minutes, treated with SDF for weeks, and treated with SDF multiple times. (**D**) Backscattered electron (BSE) and secondary electron (SE) micrographs of carious lesions treated with SDF multiple times illustrate spherulitic calcified structures within the pulp chamber (orange box). (**E**) Energy-dispersive X-ray maps show relatively lower Ca and P atomic percentages in less (obj 2) and least (obj 3) mineralized regions as compared with tubular sound dentin (obj 1). Car, caries, PC, pulp chamber; SD, sound dentin; SDF, silver diamine fluoride; TD, tertiary dentin.

consistent with previous histologic studies demonstrating tertiary dentin formation following SDF application (Gotjamanos 1996; Korwar et al. 2015; Bimstein and Damm 2018). However, further histologic studies should be done to elucidate the cellular mechanisms associated with tertiary dentin formation associated with SDF treatment.

µXRF (Fig. 4) revealed the presence of Zn along the carious surface and pulp chamber of teeth untreated and treated with SDF. To our knowledge, this is the first study to colocalize elements and contextualize these findings through correlative imaging analyses. In particular, Zn localization within the tooth structure of carious teeth treated with SDF was mapped. Zn has been demonstrated to play a role in biomineralization of tissues in teeth (Charadram et al. 2013). In the case of teeth, Zn can be introduced from exogenous routes (Cummins and Creeth 1992; Barceloux 1999). However, the observed elevated Zn is proposed to be in the reactionary dentin and predentin of carious teeth; the anatomy-specific presence could be its regulatory role in biomineralization in response to carious insult. Zn has also been identified in calcospherites of healthy teeth, suggesting its presence to be a prerequisite to tertiary dentin formation (Hietala and Larmas 1991). Higher Zn regions within the carious lesion and in the mineralized regions lining the pulp chamber and lower Zn regions observed on sound dentin may indicate a Zn-dependent biomineralization process in regions necessitating tissue repair. Zn was colocalized to regions of tertiary dentin, which was more abundant in SDF-weeks and SDF-multiple carious specimens (Fig. 5). Thus, in addition to providing a mechanical barrier to carious stimuli, SDF may be inducing an adaptive pulpal response to enhance mineral deposition by odontoblasts as a protective defense against microbial stimuli. Within sclerotic dentin situated between carious dentin and sound dentin, a higher MD profile coupled with higher levels of Zn and P and lower levels of Ca was observed. This mineralization pattern may indicate regions higher in zinc phosphate, which is less soluble than calcium phosphate (Charadram et al. 2013) and contributes to a higher MD. Within the volume of the carious lesion, Zn may be interacting with MMPs and alkaline phosphatase to promote degeneration of matrix proteins, resulting in the release of growth factors and signaling molecules and, in turn, remineralization of dentin (Okamoto et al. 2018). The localization of Zn in carious teeth is unclear and warrants exploration. These findings, however, introduce a potentially unique role that Zn may play in the pathogenesis and treatment of caries.

Overall, the results of this study indicate that the interaction of SDF with the dentin-pulp complex ultimately alters the physicochemical properties of the tooth, and these alterations contribute to the mechanism of action of SDF in caries arrest and desensitization, including tertiary dentin formation. Spatial maps of elements spanning the carious margin to the pulp illustrate the significance of the "flocking" of these elements, including trace metals that could play a role in forming mineral, which could either be biologically controlled or induced.

Author Contributions

R.M. Sulyanto, contributed to conception, design, data acquisition, analysis, and interpretation, drafted and critically revised the manuscript; M. Kang, Y. Wang, contributed to design, data acquisition, analysis, and interpretation, drafted and critically revised the manuscript; S. Srirangapatanam, J.R. Dickson, contributed to design, data analysis, and interpretation, drafted and critically revised the manuscript; M. Berger, contributed to conception, design, data acquisition, analysis, and interpretation, critically revised the manuscript; F. Candamo, contributed to design, data acquisition, and analysis, critically revised the manuscript; M.W. Ng, contributed to conception, critically revised the manuscript; S.P. Ho, contributed to conception, design, and data interpretation, drafted and critically revised the manuscript. All authors gave final approval and agree to be accountable for all aspects of the work.

Acknowledgments

The authors thank Dr. Sirine Fakra for assistance at beamline 10.3.2 and Grace Nonomura for her help with μXRF specimen preparation. The authors thank the Biomaterials and Bioengineering Correlative Microscopy Core, University of California San Francisco, for use of the MicroXCT-200 μXCT and the SIGMA 500-VP field emission electron microscope. This research used beamline 10.3.2 of the Advanced Light Source, a Department of Energy Office of Science user facility under contract DE-AC02-05CH11231.

Declaration of Conflicting Interests

The authors declared no potential conflicts of interest with respect to the research, authorship, and/or publication of this article.

Funding

The authors disclosed receipt of the following financial support for the research, authorship, and/or publication of this article: This work was supported by the Paul K. Losch Fund (R.M.S.), Harvard School of Dental Medicine Dean's Innovation Fund (R.M.S.), and Sunstar/AAPD Postgraduate Research Fellowship (M.B.). This work also was supported by the National Institute of Dental and Craniofacial Research / National Institutes of Health (R01 DE022032 to S.P.H.) and the Program in Biomineralization Studies, a joint program between the Department of Preventive and Restorative Dental Sciences (School of Dentistry) and Department of Urology (School of Medicine) at the University of California San Francisco.

ORCID iDs

M. Kang https://orcid.org/0000-0002-3188-4481
S. Srirangapatanam https://orcid.org/0000-0002-9179-3573

References

Barceloux DG. 1999. Zinc. J Toxicol Clin Toxicol. 37(2):279–292.
Bimstein E, Damm D. 2018. Human primary tooth histology six months after treatment with silver diamine fluoride. J Clin Pediatr Dent. 42(6):442–444.
Chairside guide: silver diamine fluoride in the management of dental caries lesions. 2018. Pediatr Dent. 40(6):492–517.
Charadram N, Austin C, Trimby P, Simonian M, Swain MV, Hunter N. 2013. Structural analysis of reactionary dentin formed in response to polymicrobial invasion. J Struct Biol. 181(3):207–222.
Chu CH, Lo ECM, Lin HC. 2002. Effectiveness of silver diamine fluoride and sodium fluoride varnish in arresting dentin caries in Chinese pre-school children. J Dent Res. 81(11):767–770.
Crystal YO, Marghalani AA, Ureles SD, Wright JT, Sulyanto R, Divaris K, Fontana M, Graham L. 2017. Use of silver diamine fluoride for dental caries management in children and adolescents, including those with special health care needs. Pediatr Dent. 39(5):135–145.
Crystal YO, Niederman R. 2019. Evidence-based dentistry update on silver diamine fluoride. Dent Clin North Am. 63(1):45–68.
Cummins D, Creeth JE. 1992. Delivery of antiplaque agents from dentifrices, gels, and mouthwashes. J Dent Res. 71(7):1439–1449.
Djomehri SI, Candell S, Case T, Browning A, Marshall GW, Yun W, Lau SH, Webb S, Ho SP. 2015. Mineral density volume gradients in normal and diseased human tissues. PLoS One. 10(4):e0121611.
Frencken JE, Peters MC, Manton DJ, Leal SC, Gordan VV, Eden E. 2012. Minimal intervention dentistry for managing dental caries—a review: report of a FDI task group. Int Dent J. 62(5):223–243.
Gotjamanos T. 1996. Pulp response in primary teeth with deep residual caries treated with silver fluoride and glass ionomer cement ("atraumatic" technique). Aust Dent J. 41(5):328–334.
Hietala EL, Larmas MA. 1991. Mineral content of different areas of human dentin in hypophosphataemic vitamin D–resistant rickets. J Biol Buccale. 19(2):129–134.
Horst JA, Ellenikiotis H, Milgrom PL. 2016. UCSF protocol for caries arrest using silver diamine fluoride: rationale, indications and consent. J Calif Dent Assoc. 44(1):16–28.
Kirk EE, Meyer MJ. 1992. Morphology of the mineralizing front and observations of reparative dentine following induction and inhibition of dentinogenesis in the rat incisor. Endod Dent Traumatol. 8(5):195–201.
Klinge RF. 2001. Further observations on tertiary dentin in human deciduous teeth. Adv Dent Res. 15:76–79.
Korwar A, Sharma S, Logani A, Shah N. 2015. Pulp response to high fluoride releasing glass ionomer, silver diamine fluoride, and calcium hydroxide used for indirect pulp treatment: an in-vivo comparative study. Contemp Clin Dent. 6(3):288–292.
Larmas M, Sándor GKB. 2014. Enzymes, dentinogenesis and dental caries: a literature review. J Oral Maxillofac Res. 5(4):e3.
Li Y, Liu Y, Psoter WJ, Nguyen OM, Bromage TG, Walters MA, Hu B, Rabieh S, Kumararaja FC. 2019. Assessment of the silver penetration and distribution in carious lesions of deciduous teeth treated with silver diamine fluoride. Caries Res. 53(4):431–440.
Llodra JC, Rodriguez A, Ferrer B, Menardia V, Ramos T, Morato M. 2005. Efficacy of silver diamine fluoride for caries reduction in primary teeth and first permanent molars of schoolchildren: 36-month clinical trial. J Dent Res. 84(8):721–724.
Mei ML, Ito L, Cao Y, Lo ECM, Li QL, Chu CH. 2014. An ex vivo study of arrested primary teeth caries with silver diamine fluoride therapy. J Dent. 42(4):395–402.
Mei ML, Li QL, Chu CH, Yiu CKY, Lo ECM. 2012. The inhibitory effects of silver diamine fluoride at different concentrations on matrix metalloproteinases. Dent Mater. 28(8):903–908.
Mishima H, Kozawa Y. 1998. SEM and EDS analysis of calcospherites in human teeth. Eur J Oral Sci. 106 Suppl 1:392–396.
Okamoto M, Takahashi Y, Komichi S, Cooper PR, Hayashi M. 2018. Dentinogenic effects of extracted dentin matrix components digested with matrix metalloproteinases. Sci Rep. 8(1):10690.
Pashley DH, Matthews WG. 1993. The effects of outward forced convective flow on inward diffusion in human dentine in vitro. Arch Oral Biol. 38(7):577–582.

R Core Team. 2020. R: a language and environment for satistical computing. Vienna (Austria): R Foundation for Statistical Computing. https://www.R-project.org/

Sayed M, Matsui N, Uo M, Nikaido T, Oikawa M, Burrow MF, Tagami J. 2019. Morphological and elemental analysis of silver penetration into sound/demineralized dentin after SDF application. Dent Mater. 35(12):1718–1727.

Schindelin J, Arganda-Carreras I, Frise E, Kaynig V, Longair M, Pietzsch T, Preibisch S, Rueden C, Saalfeld S, Schmid B, et al. 2012. Fiji: an open-source platform for biological-image analysis. Nat Methods. 9(7):676–682.

Seto J, Horst JA, Parkinson DY, Frachella JC, DeRisi JL. 2020. Enhanced tooth structure via silver microwires following treatment with 38 percent silver diamine fluoride. Pediatr Dent. 42(3):226–231.

Shah S, Bhaskar V, Venkatraghavan K, Choudhary P, M G, Trivedi K. 2014. Silver diamine fluoride: a review and current applications. J Adv Oral Res. 5(1):25–35.

Slayton RL, Urquhart O, Araujo MWB, Fontana M, Guzmán-Armstrong S, Nascimento MM, Nový BB, Tinanoff N, Weyant RJ, Wolff MS, et al. 2018. Evidence-based clinical practice guideline on nonrestorative treatments for carious lesions: a report from the American Dental Association. J Am Dent Assoc. 149(10):837–849.e19.

Suzuki T, Nishida M, Sobue S, Moriwaki Y. 1974. Effects of diammine silver fluoride on tooth enamel. J Osaka Univ Dent Sch. 14:61–72.

Urquhart O, Tampi MP, Pilcher L, Slayton RL, Araujo MWB, Fontana M, Guzmán-Armstrong S, Nascimento MM, Nový BB, Tinanoff N, et al. 2019. Nonrestorative treatments for caries: systematic review and network meta-analysis. J Dent Res. 98(1):14–26.

Willershausen I, Schulte D, Azaripour A, Weyer V, Briseño B, Willershausen B. 2015. Penetration potential of a silver diamine fluoride solution on dentin surfaces: an ex vivo study. Clin Lab. 61(11):1695–1701.

Yee R, Holmgren C, Mulder J, Lama D, Walker D, van Palenstein Helderman W. 2009. Efficacy of silver diamine fluoride for arresting caries treatment. J Dent Res. 88(7):644–647.

Yu OY, Zhao IS, Mei ML, Lo ECM, Chu CH. 2018. Caries-arresting effects of silver diamine fluoride and sodium fluoride on dentine caries lesions. J Dent. 78:65–71.

Zhao IS, Gao SS, Hiraishi N, Burrow MF, Duangthip D, Mei ML, Lo EC-M, Chu C-H. 2018. Mechanisms of silver diamine fluoride on arresting caries: a literature review. Int Dent J. 68(2):67–76.

Zhi QH, Lo ECM, Lin HC. 2012. Randomized clinical trial on effectiveness of silver diamine fluoride and glass ionomer in arresting dentine caries in preschool children. J Dent. 40(11):962–967.